Temperature-dependent protease LasB from *Aeromonas hydrophila* PS-1 mediates enteritis and pyroptosis in *Pelodiscus sinensis*

Siyu Chen[1,2], Zhenjia Huang[1,2], Xueqian Weng[1,2], Jiehao Xu[1], Wei Sun[1,2], Chutian Ge[1,2,*], Fa Dai[1,2,*]

[1]College of Biological and Environmental Sciences, Zhejiang Wanli University, Ningbo, Zhejiang 315100, China

[2]Institute of Animal Sex and Development, Zhejiang Wanli University, Ningbo, Zhejiang 315100, China

Funds:

This work was financially supported by the Zhejiang Provincial Top Key Discipline of Biological Engineering (ZS2023013), National Natural Science Foundation of China (32325049, U22A20529), Natural Science Foundation of Zhejiang Province (LZ25C190001), Key Research and Development Program of Ningbo (2025Z092).

Corresponding author:

Chutian Ge, Fa Dai

E-mail address: cge@zwu.edu.cn (Chutian Ge), daifa@zwu.edu.cn (Fa Dai)

uncorrected proof

Abstract: Temperature is crucial for the interaction between pathogens and hosts, especially for ectotherms, which is closely related to the occurrence of disease. Chinese soft-shelled turtle (*Pelodiscus sinensis*, *P. sinensis*), as an economically valuable aquatic species, is also an ectothermic animal. Its aquaculture industry is severely affected by pathogens. Therein, *Aeromonas hydrophila* (*A. hydrophila*) is one of the main pathogens causing bacterial diseases in *P. sinensis*. Here, we found that temperature is essential for the pathogenicity of *A. hydrophila* to *P. sinensis*. What's more, a temperature-dependent virulence factor LasB, which mediated pyroptosis of intestinal fibroblast-like cells of *P. sinensis* was identified. Through expression detection at different temperatures, it was found that the expression level of LasB was highest at 35℃. Moreover, after knockout of *lasB*, the toxicity of the bacteria to intestinal fibroblast-like cells of *P. sinensis* was decreased, with reduced cell damage and lower LDH release rate associated with pyroptosis. Transcriptomic analysis revealed that LasB knockout significantly attenuated the upregulation of pyroptosis-related genes (*GSDMA*, *NLRP3*, *IL-1β*, and *IL-18*) and inflammatory pathways in infected cells. After knockout of *lasB*, the pathogenicity of *A. hydrophila* to *P. sinensis* is significantly reduced, especially at 35℃. These results indicated that LasB played an important role in the pathogenicity of *A. hydrophila*, and its virulence is closely related to temperature.

Keywords: *Aeromonas hydrophila*, *Pelodiscus sinensis*, LasB, temperature, intestinal fibroblast-like cell, pyroptosis

Uncorrected proof

1 Introduction

Environmental factors play a pivotal role in mediating the interactions between pathogens and their hosts. Among them, temperature may influence physiological state and immune function, thereby altering their susceptibility to pathogens. In endothermic species, the thermal optimum for bacterial pathogens is aligned with the host's internal body temperature (Cascarano et al., 2021). In other ectothermic hosts, mainly in aquatic animals, drastic temperature fluctuations frequently inflict heavy losses on the aquaculture industry. For instance, from 2018 to 2023, the cumulative incidence rate of diseases in large yellow croaker (*Larimichthys crocea*) farming in Zhejiang Province has increased annually. The peak disease periods are in January to April and June to October, when temperature changes are significant. This leads to infections and large-scale fish deaths, resulting in severe economic losses for farmers (He et al., 2025). Temperature-regulated type II grass carp reovirus (GCRV-II) is the primary pathogen causing grass carp hemorrhagic disease, with mortality rates reaching up to 80% and exhibiting obvious seasonality (prevalent at 25-28℃ in summer). Among these factors, temperature serves as the key environmental factor regulating GCRV-II latent infection and reactivation. Low temperatures shift the virus from multi-tissue distribution to latency exclusively in brain tissue, while temperature elevation can activate latent virus, leading to disease recurrence (Jiang et al., 2023). For pathogens, virulence gene expression is directly tied to ambient temperature due to their varying body temperature. Temperature directly regulates growth, survival, and transmission efficiency. Notably, certain pathogens, such as *A. hydrophila*, exhibit venhanced expression of virulence genes within specific temperature ranges (Abdella et al., 2024). A number of *Aeromonas* virulence genes, such as those for *aerolysin* (aer), cytotoxic enterotoxin (act), and the type III secretion system (T3SS), have been shown to be temperature-dependent (Pattanayak et al., 2020). Therefore, temperature serves as a critical factor in aquaculture. Reasonably controlling and utilizing temperature, in combination with other management measures, can effectively prevent and control the occurrence of aquatic diseases and improve the efficiency of aquaculture.

Uncorrected proof

The Chinese soft-shelled turtle *P. sinensis* is an amphibious oviparous reptile and a species of soft-shelled freshwater turtle in the genus *Pelodiscus* (Wu et al., 2024). The *P. sinensis* is an important and high-quality aquaculture species in China. In 2024, the breeding output reached 498,000 tons, with a value of over 20 billion yuan (Xiang et al., 2025; Li et al., 2025). The development of *P. sinensis* breeding is rapid, with increasing levels of scale and intensification. As a poikilothermic animal, its growth is significantly influenced by water temperature. The optimal growth temperature range is 25-35℃, with the most suitable temperature being 28-30℃ (Chen et al., 2020). Abrupt fluctuations in water temperature often lead to disease outbreaks in *P. sinensis*. For example, a rapid rise in temperature during the transition from spring to summer, combined with intensive aquaculture practices, frequently results in large-scale mortality of *P. sinensis*.

The common bacterial diseases in *P. sinensis* are closely related to *A. hydrophila*. *A. hydrophila* is a Gram-negative opportunistic pathogen and is one of the main pathogens causing a variety of diseases (Abdella et al., 2023). For example, red neck disease (Lin et al., 2005), branchial gland inflammation (Dai et al., 2025), and ulcerative dermatitis (Chen et al., 2017) all caused by *A. hydrophila* alone or in combination with other bacteria. These diseases caused symptoms such as redness, swelling, ulcers, and necrosis in *P. sinensis*, seriously affecting their growth and health. In *A. hydrophila*, virulence factors such as enterotoxins (De Silva LADS et al., 2021), hemolysins (Awna et al., 2018), aerolysin (Fikrif et al., 2022), Shiga toxin (Thomas et al., 2020) and extracellular enzymes (Fernández-Bravo et al., 2020) have been identified. However, the association between diseases in the *P. sinensis* and the virulence factors of *A. hydrophila* remains unknown, and the role of temperature is also unclear. Our previous work showed that the primary colonization site of *A. hydrophila* in infected turtles is the intestine, where it elicits intestinal inflammation and pyroptosis of fibroblast-like cells (Dai et al., 2026). However, virulence factors of *A. hydrophila* responsible for these immune responses remains unclear. Previous studies have found that, the elastase LasB in *Pseudomonas aeruginosa* could directly cleave and activate IL-1β, enhancing the recruitment of neutrophils and the

Uncorrected proof

inflammatory response, leading to the destruction and damage of lung tissue (Sun et al, 2020). What's more, the cysteine protease SpeB in *Streptococcus* could induce pyroptosis by cleaving GSDMA, indirectly activating the host's immune system, promoting the inflammatory response, and helping the host resist bacterial infections (Deng et al., 2022). The above studies indicated that, bacterial proteases play an extremely important role in the physiological functions and pathogenic processes of bacteria. They can destroy the tissues and cells of the host, promote bacterial invasion and spread, or regulate the infection process by activating or inhibiting the host's immune response.

This study employed a strain of *A. hydrophila* (PS-1), previously isolated by our team from the intestines of diseased *P. sinensis*, to investigate the influence of temperature on pathogen-host interactions. We demonstrated that the LasB protease of *A. hydrophila* was a temperature-dependent virulence factor that was involved in inflammatory intestinal diseases in *P. sinensis* by inducing pyroptosis in intestinal fibroblast-like cells.

2 Materials and methods

2.1 Bacterial strains, culture conditions and chemicals

The *A. hydrophila* strain PS-1 used in this study was isolated from diseased *P. sinensis*. PS-1 was cultured at 28℃in Luria-Bertani (LB) medium consisting 10 g/L tryptone, 5 g/L yeast extract, and 10 g/L NaCl in sterile water. *Escherichia coli* DH5α, S17λπ and BL21 (DE3) were purchased from Cowin Biotech (China) and cultured in LB medium at 37℃. The plasmid vectors utilized in this experiment were mainly pMD19-T (Taraka Corporation, Japan), pET-28a (preserved in our laboratory), and pDM4 (preserved in our laboratory). The antibiotics used in this study include ampicillin (Amp), kanamycin (Kana), and chloramphenicol (Cm), which were purchased from Shanghai Sangon Biotech.

2.2 DNA manipulation and plasmid construction

2.2.1 Construct the expression strain BL21/pET-28a-LasB

Using PS-1 genomic DNA as the template, the *lasB* gene was amplified with primers LasB-F (5'-cagcaaatgggtcgcggatccATGTCCAGACCGATCCCCTC-3') and LasB-R (5'-ctcgagtgcggccgcaagcttTCAGTCAATCCCGTTGTTGTAGAG-3'). The

Uncorrected proof

PCR product was cloned into the pMD19-T vector and transformed into *E. coli* DH5α competent cells. The positive construct was sequenced by Sangon Biotech Co., Ltd, and the corresponding strain was preserved.

Plasmids were extracted from DH5α/pMD19-T-LasB and DH5α/pET-28a, then double-digested with *BamH* I and *Hind* III at 37℃ for 3 h. The digested lasB fragment and pET-28a vector were gel-purified and ligated at 16℃ overnight. The ligation product was transformed into DH5α competent cells, and positive clones were screened by colony PCR using LasB-F/LasB-R primers and confirmed by sequencing. The verified plasmid was extracted and transformed into *E. coli* BL21 (DE3) competent cells to construct the expression strain BL21/pET-28a-LasB .

2.2.2 Knockout of *lasB*

Primers UpF, UpR, LowF, and LowR were designed for the *lasB* gene of PS-1 and were named as follows: ΔLasB UpF (5'-GTCATCTAGATGGCCATCCTCAGTCGTG-3'), ΔLasB UpR (5'-TGGTAGACAGGTTTCGTAGTAATCCCTG-3'), ΔLasB LowF (5'-CGATCTGCACGACTCTGGCTCTACAACC-3'), and ΔLasB LowR (5'GTCAGTCGACCAGATCGCCAAACAGCTT-3'). Through PCR reactions, the ΔLasB Up and ΔLasB Low fragments were constructed separately. The purified and recovered Up and Low fragments were used as templates, and overlapping PCR was performed using the same method with primers UpF/LowR. Subsequently, agarose gel electrophoresis was conducted. The overlapping PCR products of the desired fragment size were purified and recovered for later use. The ΔLasB fragment was double-digested with the restriction enzymes *Xba* I and *Sal* I. Simultaneously, the pDM4 suicide plasmid was also double-digested with the same restriction enzymes. After purification and recovery of the digestion reaction mixtures, ligation was performed, and the product was transformed into *E. coli* S17λπ by heat shock. The transformants were spread on LB (Cm, 30 μg/mL) plates. Single colonies were subjected to PCR detection to obtain S17λπ/pDM4-ΔLasB.

The donor strain was prepared by inoculating S17λπ/pDM4-ΔLasB into 5 mL of liquid LB (Cm, 30 μg/mL) medium and culturing at 28℃ for 12 h. The recipient strain was prepared by inoculating PS-1 into 5 mL of liquid LB (Km, 30 μg/mL) medium and culturing at 28℃ for 12 h. The donor and recipient strains were mixed at the radio of 1:1, and spotted to the LB agar medium. After 48 h, the bacterial plaques were

Uncorrected proof

harvested, serially diluted, and spread onto LB plates containing 30 μg/mL Km and 300 μg/mL Cm. The successful single crossover strains were detected by PCR. The suspension of the successfully obtained single crossover strains was then inoculated into 5 mL of fresh LB medium without antibiotics and cultured overnight. The culture was then serially diluted, and 10^{-1}, 10^{-2}, 10^{-3}, and 10^{-4} dilutions were spread on LBS (containing 12% sucrose) (Km, 30 μg/mL) solid plates. Single colonies that grew were detected by PCR to screen for mutant strains ΔLasB with the desired fragment size. Finally, the constructed mutant strain ΔLasB was confirmed to be correct by resistance testing and sequencing.

2.3 Expression and purification of recombinant LasB

Overnight culture of *E. coli* BL21/pET28a-LasB was inoculated into 100 mL LB medium with Km and cultured at 37℃ until the OD_{600} reached 0.5. Isopropyl-β-D-thiogalactopyranoside was added into the culture at a working concentration of 0.4 mM to induce the expression of LasB and the induction process lasted for 6 h at 28℃. Then, the cells were harvested by centrifuging at 8000×g for 10 min. Cells were precipitated and used for the purification of recombinant protein. Recombinant His-tagged LasB was purified using Ni-NTA Sepharose column (Roche, Shanghai). The recombinant protein was determined by 12% SDS polyacrylamide gel electrophoresis (SDS-PAGE) and the concentration of recombinant protein was measured using the BCA Protein Assay Kit (Sangon, China).

2.4 Antibody preparation

Purified recombinant LasB protein was used as the immunogen to immunize healthy 3-month-old rabbits. For the primary immunization, 200 μg of purified LasB protein was thoroughly emulsified with an equal volume of Complete Freund's Adjuvant (CFA) to form a water-in-oil emulsion, which was then administered via multipoint subcutaneous injection on the back. On day 7 after the initial immunization, a booster immunization was performed: 200 μg of purified LasB protein was thoroughly mixed with an equal volume of IFA, and administered using the same multipoint subcutaneous injection method on the back. After an interval of 7 days, the booster immunization protocol was repeated once more. Seven to ten days after the final immunization, blood was collected from the rabbit marginal ear vein. The serum was separated, and crude IgG was purified by Protein A/G affinity chromatography to obtain the LasB polyclonal antibody. The prepared antibody

Uncorrected proof

samples were aliquoted and stored at -80℃ in an ultra-low temperature freezer to avoid repeated freeze-thaw cycles, for subsequent experimental use.

2.5 Western blot analysis

A total of 30 μg of protein from each sample was separated through SDS-PAGE then transferred to a 0.45 mm pore nitrocellulose membrane with an Enhanced ChemiLuminescence (ECL) Semidry Blotter (Amersham Biosciences, USA). The membrane was blocked with 5% skim milk in TBST (20 mM Tris-HCl, 150 mM NaCl, and 0.05% Tween-20) at 37℃ for 1 h. The membranes were then incubated with polyclonal antibodies diluted to 1:400 in 5% skimmed milk at 4℃ for 12 h. After washing the membrane for three times with TBST for 10 min, the membrane was subsequently incubated with diluted goat-anti mouse or goat-anti rabbit IgG (Sangon, China) diluted to 1:3000 at room temperature for 1 h. The membrane was further washed with TBST for three times and incubated in Western Lightning-ECL substrate (Yamei, China) prior to exposure to a X-OMAT AR X-ray film (Eastman Kodak, USA). Band density was analyzed with ImageJ, and protein expression levels were normalized to that of RNAP control.

2.6 Sequence analysis

The sequences of *lasB* genes were analyzed using the BLAST algorithm at the National Centre for Biotechnology Information (http://www.ncbi.nlm.nih.gov/blast). The deduced amino acid sequences were analyzed using the Expert Protein Analysis System (http://www.expasy.org/). The molecular mass (MM) and theoretical isoelectric point(pI) were calculated by the Protparam tool (http://www.expasy.ch/tools/protparam.html). Domains in the amino acid sequence were detected using the simple modular architecture research tool (SMART) program (http://www.smart.emblheidel bergde/). The neighborjoining phylogenetic tree was constructed using Mega 4.0 program with 1000 bootstraps.

2.7 Real-time reverse transcription PCR (RT-PCR)

The expression of the *lasB* in PS-1 cultured at different temperatures was detected by RT-PCR. Total RNA was extracted from the PS-1 using Bacterial RNA Isolation kit (Omega, USA). RT-PCR was carried out in an ABI 7500 realtime detection system (Applied Biosystems) by using the SYBR ExScript RT-PCR kit (Takara, China). The primers used for RT-PCR of *lasB* were RTLasBF

Uncorrected proof

(5'-GGCCACCAACTACTACCACATGAGCG-3') and RTLasBR (5'-GCCTCGTTGCGGTTGCTGGCATA-3'). Each assay was performed in triplicate with the 16S rDNA as a reference control. The primers used for the RT-PCR of 16S rDNA were 933F (5′-GCACAAGCGGTGGAGCATGTGG-3′) and 16SRTR1 (5′-CGTGTGTAGCCCTGGTCGTA-3′). Dissociation analysis of the amplified product was performed at the end of each PCR to confirm that only one PCR product was amplified and detected. The method of $2^{-\Delta\Delta CT}$ was used to analyze the relative mRNA level of the *lasB*.

2.8 Growth curve measurement

To determine whether the delection of *lasB* affected the growth of PS-1, the OD_{600} values of PS-1 and ΔLasB at different culture times were measured, respectively. Briefly, a single colony of PS-1 and ΔLasB was picked and separately grown in LB medium without any antibiotics at 28℃ for 12 h. The cell density of each culture was measured at 1 h interval at 600 nm by an UV-Vis spectrophotometer (Beckman) and the experiment was repeated three times.

2.9 Primary culture of intestinal fibroblast-like cells in *P. sinensis*

The intestinal fibroblast-like cell culture protocol for *P. sinensis* was adapted from our established methodology for cardiac cell line derivation in this species (Guo H et al., 2016). Under the stereomicroscope, sterile dissection was performed on the *P. sinensis* embryos at stage 20. After the intestinal tissue was completely removed, it was washed three times with DPBS to remove other tissue impurities. The intestinal tissue was minced with sterile surgical scissors and digested with 0.25% trypsin-EDTA (1:3 w/v, 28℃, 30 min). Digestion was terminated by adding DMEM complete medium (10% FBS). The digestate was filtered through 100-μm nylon mesh and centrifuged (250 g, 8 min). Cell pellets were resuspended in complete medium, followed by repeat centrifugation (200 g, 5 min) after gentle pipetting. The final suspension was seeded into culture flasks and maintained at 30℃ with 5 % CO_2.

2.10 Cell infection pattern of PS-1

Primary fibroblast-like cells isolated from the intestine of *P. sinensis* were seeded to reach 90 % confluency. PS-1 and ΔLasB was then inoculated into the cells at a multiplicity of infection of 1 (MOI = 1). Cells were observed at designated post-infection time points: 0 h (pre-infection control), 3 h, 6 h. After infection, the cells were washed with DPBS for 10 min, then immersed in electron microscopy

Uncorrected proof

fixative. They were fixed in the dark at room temperature for 20 min and then transferred to 4℃ for storage and transportation to the company for scanning electron microscopy imaging.

2.11 Infection experiment of *P. sinensis*

Activated PS-1 and ΔLasB were inoculated into LB medium and cultured to an OD_{600} of 1.0. After centrifugation, the bacterial pellets were resuspended in 2 L of sterile physiological saline. Individual *P. sinensis* weighing 30-50 g were placed in rectangular transparent plastic containers with a capacity of 5 L (3 individuals per group) and immersed separately in 2 L of sterile physiological saline containing PS-1 and ΔLasB at a final bacterial concentration of 1.0×10^7 CFU/mL, with sterile physiological saline as the control. Temperature treatments were conducted simultaneously at 28℃ and 35℃. Small intestine tissues of *P. sinensis* were collected at 3 days post-infection for subsequent experiments.

2.12 Determination of mortality rate

Individual *P. sinensis* weighing 6-12 g were placed in rectangular transparent plastic containers with a capacity of 5 L (40 individuals per group) and immersed separately in 2 L of sterile physiological saline containing PS-1 and ΔLasB at a final bacterial concentration of 1.0×10^7 CFU/mL, with sterile physiological saline as the control. Temperature treatments were conducted simultaneously at 28℃ and 35℃. The survival numbers of *P. sinensis* in each group were recorded over 11 days to quantify the mortality rate.

2.13 Histological analysis

Small intestine tissues of *P. sinensis* were collected, fixed in 4% paraformaldehyde, embedded in paraffin, cut into sections, and placed on adhesion microscope slides. Sections were subjected to H&E according to standard procedures. Stained tissue sections were imaged by light microscopy (Olympus BX53) with CellSens software.

2.14 Determination of lactate dehydrogenase (LDH) release rate

The supernatants from the cell treatments in section 2.11 were collected and incubated with the LDH detection working solution from the Lactate Dehydrogenase Cytotoxicity Assay Kit (Beyotime, China) at room temperature (25℃) in the dark for 30 min. The absorbance was then measured at 490 nm.

2.15 Determination of motility and hemolytic activity

Uncorrected proof

PS-1 and ΔLasB were streaked on LB agar plates, respectively. Single colonies were picked and inoculated into LB medium without antibiotics and incubated in a shaker at 28℃ until the OD_{600} value reached 0.5. Five microliters of each culture was spotted onto LB plates containing 0.3% agar and 5% sheep blood agar plates, respectively, and incubated in an incubator at 28℃ for more than 48 h.

2.16 Immunofluorescence

Paraffin sections were deparaffinized and rehydrated (xylene, 30 min; xylene: ethanol 1:1, 10 min; ethanol, 3 min; 90% ethanol, 3 min; 70% ethanol, 3 min; 50% ethanol, 3 min; water, 3 min) before immersion in 10 mM sodium citrate buffer for 20 min at 95℃ for antigen retrieval. After blocking for 1 h in blocking solution (10% normal donkey serum, 3% bovine serum albumin, and 0.3% Triton X-100) at room temperature, sections were incubated overnight at 4℃ with primary antibodies. The primary antibodies used in this analysis included rabbit anti-Caspase-1 (1:300) and rabbit anti-GSDMA (1:300). The sections were then washed 3 times (10 min each time) with PBST, followed by incubation with secondary antibody IgG-488 (1:250, Invitrogen) for 2 h at room temperature in a dark environment, and further washing. Nuclei were stained with 4′,6-diamidino-2-phenylindole. Fluorescent imaging was conducted via NIS-Elements AR 4.20.00 software under 10 × magnification in a laser scanning confocal microscope (A1Plus, Nikon). Acquired images were manipulated using the rotation, crop, and brightness in only a linear manner.

2.1.7 RNA-seq and DEG analysis

P. sinensis intestinal fibroblast-like cells were infected with *A. hydrophila* wild-type strain PS-1 (WT) or the ΔLasB mutant strain (KOL) at a multiplicity of infection (MOI) of 1. Cells were collected at 3 h and 6 h post-infection, with uninfected cells serving as the negative control (NC). Total RNA was extracted from the collected samples, and libraries were constructed by Novegene (China). Paired-end sequencing (150 bp) was performed using the Novaseq-PE150 (China).

Raw RNA sequencing (RNA-seq) reads were quality-checked and filtered using fastp (v.0.23.2) (Chen et al., 2018). Expression quantification was conducted using the new Tuxedo pipeline (Pertea et al., 2016): reads were aligned to the *P. sinensis* reference genome using HISAT2 (v.2.2.1) (Kim et al., 2015), and transcript quantification was performed using StringTie (v.2.2.1) (Pertea et al., 2015). Gene-level expression values were calculated using tximport (v.1.28.0) (Soneson et

Uncorrected proof

al., 2016). To account for variations across samples, fragments per kilobase of transcript per million mapped reads (FPKM) were normalized using a scaling method based on the trimmed mean of M values (TMM), under the assumption that most genes maintain consistent expression across samples.

Differentially expressed genes (DEGs) were identified using thresholds of |log2 fold change (FC)| > 0.5 and *p*-value < 0.05. Gene ontology (GO) and Kyoto encyclopedia of genes and genomes (KEGG) enrichment analyses of DEGs were performed to identify significantly enriched biological processes and pathways. Heatmaps were generated to visualize the expression patterns of the top 50 DEGs and pyroptosis-related genes across all groups.

2.18 Statistical analyses

Statistical analyses were performed by using GraphPad Prism (GraphPad Software). Standard deviation was used to reflect the dispersion of multiple independent variables relative to the mean. Unpaired two-tailed Student's t-tests were conducted for the single comparison of two groups. Two-way analysis of variance (ANOVA) was used for analysis of experiments with multiple groups and multiple independent variables, and one-way ANOVA was used for analysis of multiple groups with a single independent variable. All data are representative of at least three independent experiments and presented as the mean ± SD. Statistical significance was defined as $p > 0.05$, not significant (n.s.); $*p < 0.05$; $**p < 0.01$; and $***p < 0.001$.

3 Results

3.1 **Sequence analysis of LasB**

A comprehensive analysis of the LasB protease from PS-1 was conducted to elucidate its evolutionary relationships and structural characteristics in comparison to homologs from other clinically and environmentally significant bacterial pathogens. Multiple sequence alignment of the PS-1 LasB protein with LasB sequences from various bacterial genera, including *Shewanella denitificans* (WP_011497052.1), *Pseudomonas aeruginosa* (WP_058135975.1), *Bowanella denitificans* (WP_102797951.1), *Aeromonas salmonicida* (HGY1009356.1), *Aeromonas sp.* (S41-2, WP_270810851.1; BC14, WAF95052.1), *Photobacterium sp.* (WP_330961119.1), *Vibrio cholerae* (WP_161418048.1), *Bacterioplanes sanyensis*

Uncorrected proof

(WP_189387869.1), *Thalassomonas haliotis* (WP_274050184.1), *Saccharospirillum salsuginis* (WP_229805478.1), revealed several key findings. Among these, the sequence conservation within the M23 peptidase domain (241-340 aa) reached 70%, while the sequence similarity in other regions was relatively low, which underscored their indispensable role in the enzymatic mechanism (Fig. 1A and 1B). A phylogenetic tree was constructed based on the aligned LasB protein sequences using the Maximum Likelihood method. The resulting tree clearly delineated distinct clades corresponding to bacterial classes and families. As expected, the PS-1 LasB sequence robustly formed a well-supported clade with other *Aeromonas* species (Fig. 1C). Furthermore, structural prediction of the above sequences using AlphaFold3 revealed that the LasB proteins maintain a similar overall conformation. Particularly, the M23 peptidase domain formed a highly aligned and superimposed structure, which is a typical structural characteristic of the M23 peptidase family (Fig. 1D). Sequence analysis demonstrated that while the PS-1 LasB protease shared a conserved catalytic core with its homologs, it possessed unique sequence and structural features that likely underlie its specific functional role in the biology and pathogenicity of *Aeromonas hydrophila*.

uncorrected proof

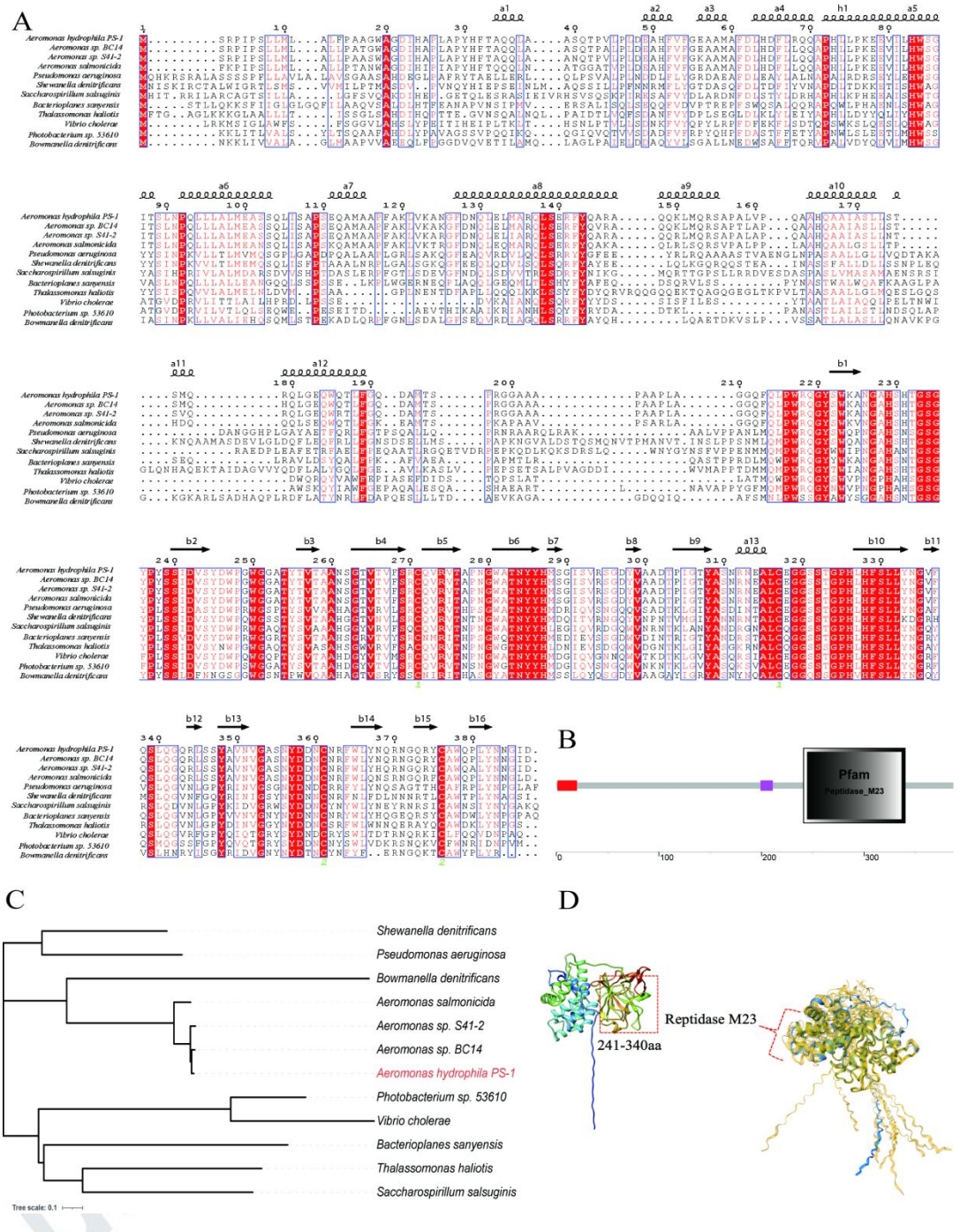


Fig. 1 Sequence analysis of LasB. A: Several sequence alignment of several bacteria LasB proteins. *Shewanella denitificans* (WP_011497052.1), *Pseudomonas aeruginosa* (WP_058135975.1), *Bowanella denitificans* (WP_102797951.1), *Aeromonas salmonicida* (HGY1009356.1), *Aeromonas sp.* S41-2, (WP_270810851.1), *Aeromonas sp.* BC14 (WAF95052.1), *Photobacterium sp.* (WP_330961119.1), *Vibrio cholerae* (WP_161418048.1), *Bacterioplanes sanyensis* (WP_189387869.1), *Thalassomonas haliotis* (WP_274050184.1), *Saccharospirillum salsuginis* (WP_229805478.1). B: Domain of PS-1 LasB. C: Phylogenetic

Zoological Research

analysis of several bacteria LasB proteins. D: Structural modeling and alignment of several bacteria LasB proteins.

3.2 LasB upregulated by *P. sinensis* intestinal protein induction

To explore the expression pattern of LasB in PS-1 under the induction of *P. sinensis* intestinal protein, we inoculated 100 μL of PS-1 into 100 mL of fresh LB medium and incubated it at a constant temperature of 28℃. After the OD_{600} value reached 0.5, we added 2 mL of *P. sinensis* intestinal protein for induction treatment. We collected 6 mL of bacterial broth at 0 h, 1 h, 2 h, and 3 h post-induction to extract bacterial secretions and total protein solutions for subsequent experiments. Following the procedures outlined in section 2.6, western blot analysis was conducted on the secretions and total protein solutions from each group to detect the expression of the LasB, which is predicted to be 42.5 kDa in size. The results showed that in the total protein, the expression of LasB gradually increased with the duration of intestinal protein induction treatment, but there were no statistically significant differences (Fig. 2A). In the secretions, the LasB band appeared at 35 kDa, and its secretion increased with the duration of intestinal protein induction treatment, reaching the highest level after 3 h of induction, with statistically significant differences (Fig. 2B). This indicated that LasB was a virulence factor for the *P. sinensis* and its expression was upregulated under intestinal protein induction.

Due to the discrepancy in the size of the LasB between the total protein and the secretions, we hypothesized that the LasB undergoed cleavage when secreted outside the cell. To verify this hypothesis, we inoculated 100 μL of PS-1 into 30 mL of fresh LB medium and incubated it at a constant temperature of 28℃ until the OD_{600} value reached 0.5, then extracted bacterial secretions and total protein solutions for western blot analysis. The results indicated that LasB was a secreted protein, detectable in both total protein and secretions, but the protein band in the secretions was around 35 kDa (Fig. 2C). LC/MS analysis showed that two annotated sequences were aligned with LasB. The peptide segment diagrams represented the two annotated sequences "QQAPHLLPK" and "LVKANGFDNQLELMAR" (Fig. 2D). This result confirmed that the 35 kDa band was indeed the LasB, suggesting that LasB did undergo protein

Uncorrected proof

cleavage when secreted from PS-1. This finding provided direction for future research, which can further verify the protein cleavage sites.

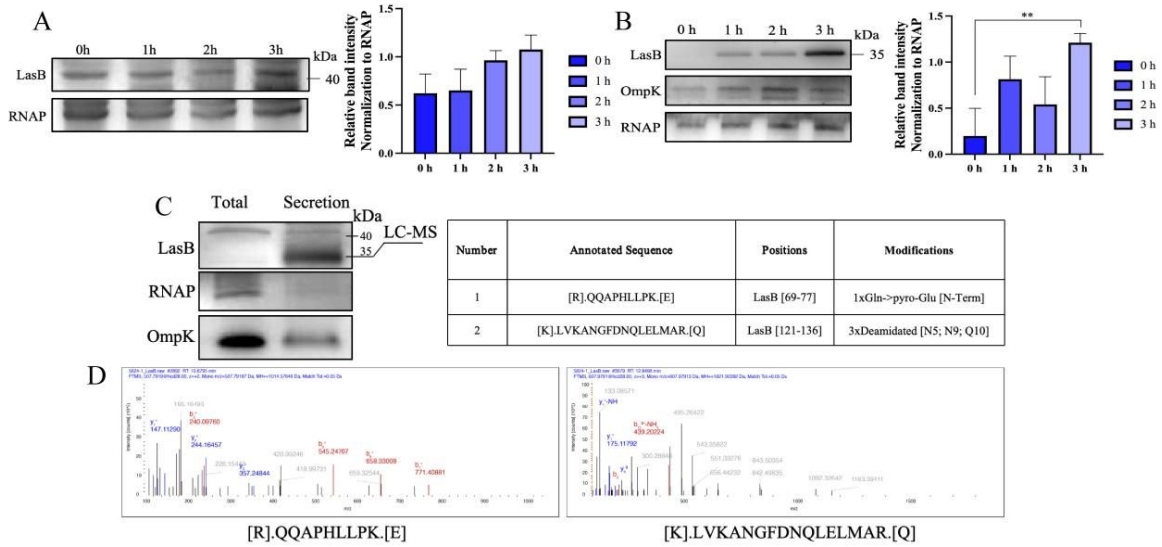


Fig. 2 LasB was a host-inducible secreted protein. A: Protein expression levels of LasB in total proteins of PS-1 treated with *P. sinensis* intestinal protein at different treatment times. B: Protein expression levels of LasB in the secreted proteins of PS-1 treated with *P. sinensis* intestinal protein at different treatment times. C: Western blot analysis of LasB in total and secreted proteins of PS-1. D: Mass spectrometry of LasB cleavage fragments. RNAP, anti-*E. coli* RNA polymerase antibody, used as the insider. OmpK, outer membrane protein K, used the control for secretory proteins. $0.01 < **p < 0.05$.

3.3 LasB was a temperature-dependent secreted protein

To further determine whether LasB was a temperature-dependent virulence factor, we inoculated 100 μL PS-1 into 30 mL of fresh LB medium. Based on the aquaculture water temperatures at which *P. sinensis* were prone to disease, the following temperature gradients were set: 22°C, 28°C, 30°C, 32°C, 35°C, 37°C, and 39°C. After incubation for 9 h, 2 mL of bacterial suspension was collected from each temperature, with three replicates, and bacterial RNA was extracted.The remaining broth was used to extract bacterial secretions and total protein solutions for subsequent experiments. According to the procedure in section 2.5, qPCR was used to detect the mRNA expression of the *lasB* cultured at different temperatures. The results revealed that *lasB* transcript levels rose markedly with temperature, reaching a maximum at 35℃ with 3.3-fold higher than 28℃, demonstrating that LasB was a temperature-dependent factor (Fig. 3A). Following the procedures outlined in section

Uncorrected Proof

2.6, we performed western blot analysis on the secretions and total protein solutions from each group to detect the protein expression of the LasB. As the temperature increased, the protein expression of LasB in the total proteins of PS-1 gradually decreased, with statistically significant differences in protein expression among the groups (Fig. 3B). In the secretions, the protein expression of LasB significantly increased at 35℃, which was consistent with the mRNA level expression. The secretion of LasB was significantly enhanced at 35℃ (Fig. 3C). These results demonstrated that LasB was a temperature-dependent virulence factor, with the highest expression at 35℃.

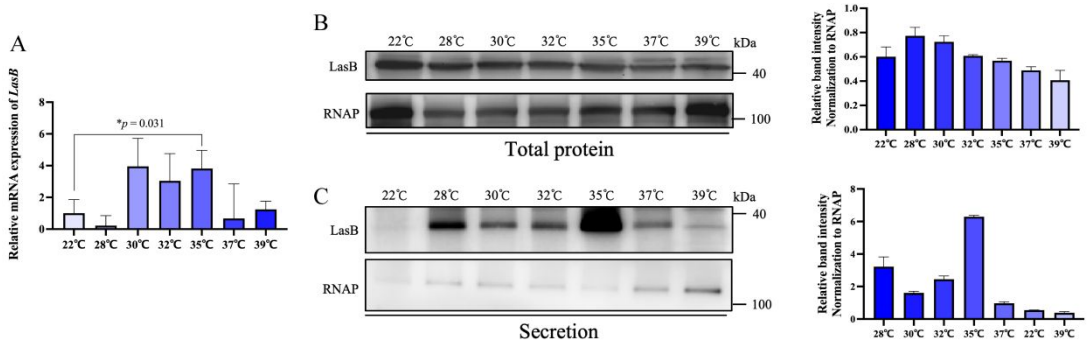


Fig. 3 LasB was a temperature-dependent secreted protein. A: The mRNA expression level of *lasB* induced by temperature gradients. B: The protein expression level of LasB in total proteins of PS-1 induced by temperature gradients. C: The protein expression level of LasB in the secreted proteins of PS-1 induced by temperature gradients. **p* <0.05.

3.4 Knockout of *lasB*

After confirming that LasB was a temperature-dependent virulence factor, we constructed the *lasB* knockout strain ΔLasB according to the procedures in sections 2.2.2 and 2.7. Based on the open reading frame (ORF) of *lasB* and following the overlap principle, we designed an in-frame complete knockout (Fig. 4A). The successful knockout of the *lasB* was confirmed at both the nucleic acid and protein levels by PCR (Fig. 4B) and WB (Fig. 4C), respectively. ΔLasB failed to amplify the complete *lasB* segment and did not express the LasB protein, indicating that we successfully knocked out the *lasB* in PS-1. We then further investigated whether the *lasB* had any pleiotropic effects on the growth, motility, or virulence-related phenotypes of PS-1. The growth curve showed that the growth rate of ΔLasB during

Uncorrected Proof

471 the logarithmic phase was similiar with PS-1, reaching the same maximum biomass as
472 the wild type around 12 h, confirming that the knockout of the *lasB* did not hinder the
473 growth of PS-1 (Fig. 4D). There was no statistically significant difference in the
474 migration diameter between the PS-1 and ΔLasB, indicating that the motility of
475 ΔLasB was not impaired (Fig. S1). On the 5% sheep blood agar plates, a clear zone of
476 hemolysis surrounded the colonies of the PS-1, whereas the colonies of ΔLasB
477 showed significantly reduced hemolytic activity due to the absence of LasB elastase,
478 resulting in a less distinct hemolytic zone (Fig. S1). To assess pathogenicity,
479 individual *P. sinensis* weighing 6-12 g were placed in rectangular transparent plastic
480 containers with a capacity of 5 L (40 individuals per group) and immersed separately
481 in 2 L of sterile physiological saline containing PS-1 and ΔLasB at a final bacterial
482 concentration of 1.0×10^7 CFU/mL. To evaluate the temperature-dependent
483 pathogenicity of LasB, we monitored the survival rates of *P. sinensis* following
484 infection with PS-1 or ΔLasB at 28℃ and 35℃ (Fig. 4E). Both the NC and 28℃
485 ΔLasB-infected groups maintained a high survival rate of 97.5%, indicating minimal
486 pathogenicity of the mutant at this temperature. At 28℃, infection with PS-1 slightly
487 reduced the survival rate to 87.5%. However, the pathogenicity of PS-1 was
488 significantly exacerbated under high-temperature stress; the 35℃ PS-1 group
489 exhibited the highest mortality, with the survival rate dropping to 77.5%. Importantly,
490 knocking out LasB partially attenuated this heat-exacerbated virulence, as the 35℃
491 ΔLasB group maintained a higher survival rate of 80%. Collectively, these survival
492 kinetics demonstrate that PS-1 pathogenicity is highly temperature-dependent and that
493 LasB serves as a crucial virulence factor contributing to lethality in *P. sinensis*.

Uncorrected proof

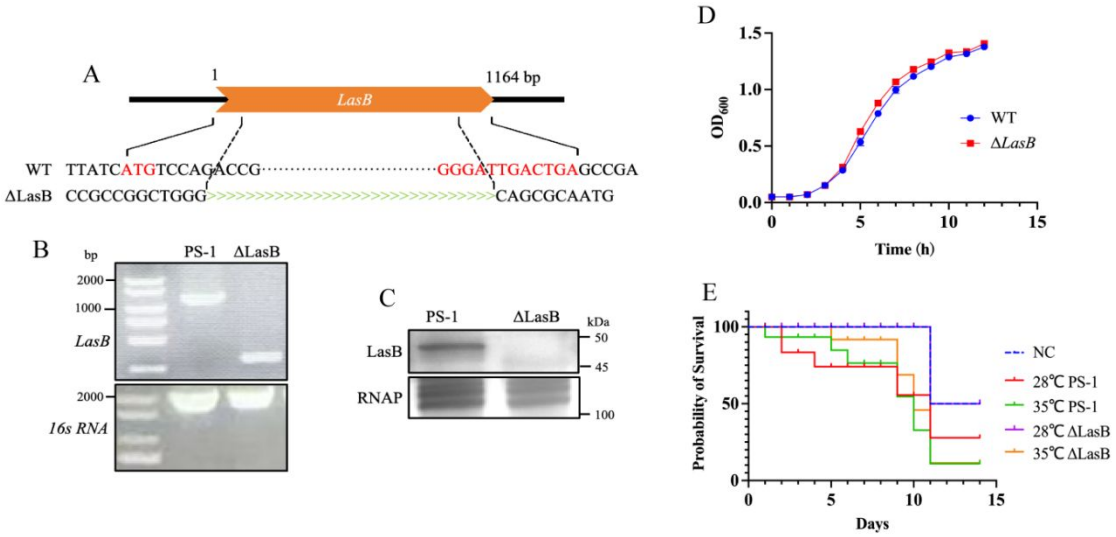


Fig. 4 Construction and characterization of ΔLasB. A: In-frame complete knockout of *lasB*. B: PCR verification of *lasB* at the nucleic acid level between PS-1 and ΔLasB C: Western blot verification of LasB at the protein level between PS-1 and ΔLasB. D: Growth curves of PS-1 and ΔLasB. E: Assessment of the survival rate of *P. Sinensis* infected with PS-1 and ΔLasB at different temperature.

3.5 Temperature-dependent pathogenicity of the LasB to *P. sinensis*

To evaluate the temperature-dependent pathogenicity of LasB, we performed infection assays using the PS-1 and ΔLasB strains at 28℃ and 35℃. At 3 days post-infection, H&E staining were performed to assess tissue damage. The uninfected temperature-control groups exhibited normal morphology, with intact intestinal architecture and only mild plastron redness at 35℃. In stark contrast, PS-1 infection at 35℃ triggered a severe inflammatory response. Macroscopically, *P. sinensis* developed multiple ulcerative lesions and severe plastron erythema, accompanied by marked intestinal atrophy. Histologically, PS-1 induced massive intestinal inflammation, characterized by disrupted tissue structure, severe mucosal and glandular edema, and detachment of the villous epithelium. Notably, these pronounced inflammatory pathologies were significantly alleviated in the ΔLasB-infected group. *P. sinensis* infected with the mutant strain exhibited only slight superficial inflammation, and their intestinal tissues retained relatively intact cellular morphology with a markedly reduced inflammatory response (Fig. 5A and 5B). Together, these results demonstrate that LasB is a crucial temperature-dependent virulence factor responsible for driving severe inflammatory damage in *P. sinensis*.

Uncorrected Proof

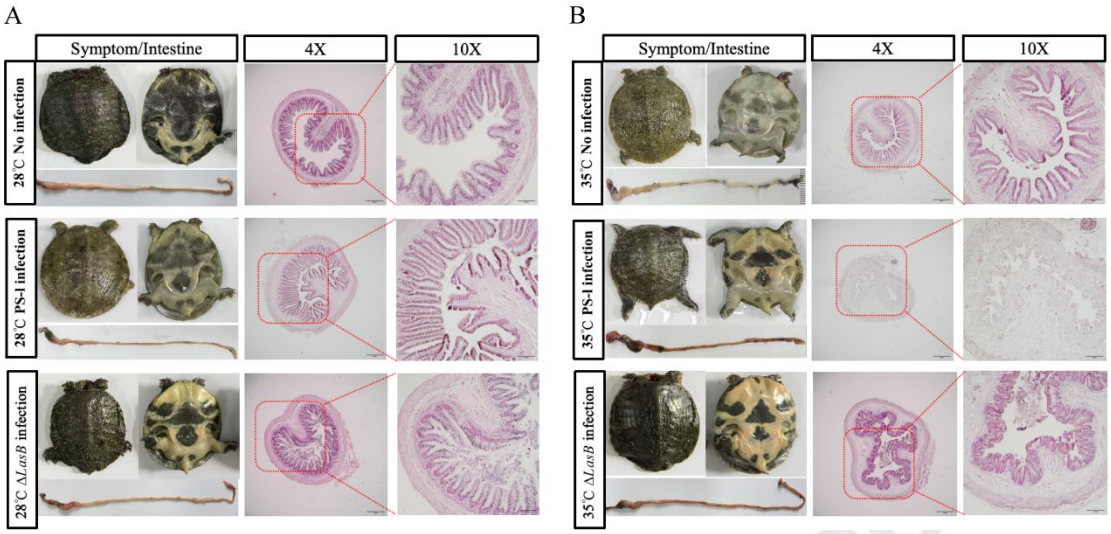


Fig. 5 Pathogenicity of the LasB to *P. sinensis*. A and B: Histological observation of intestinal tissues three days post-infection with PS-1 and ΔLasB to further confirm pathogenic effects. Scale bar, 100 μm.

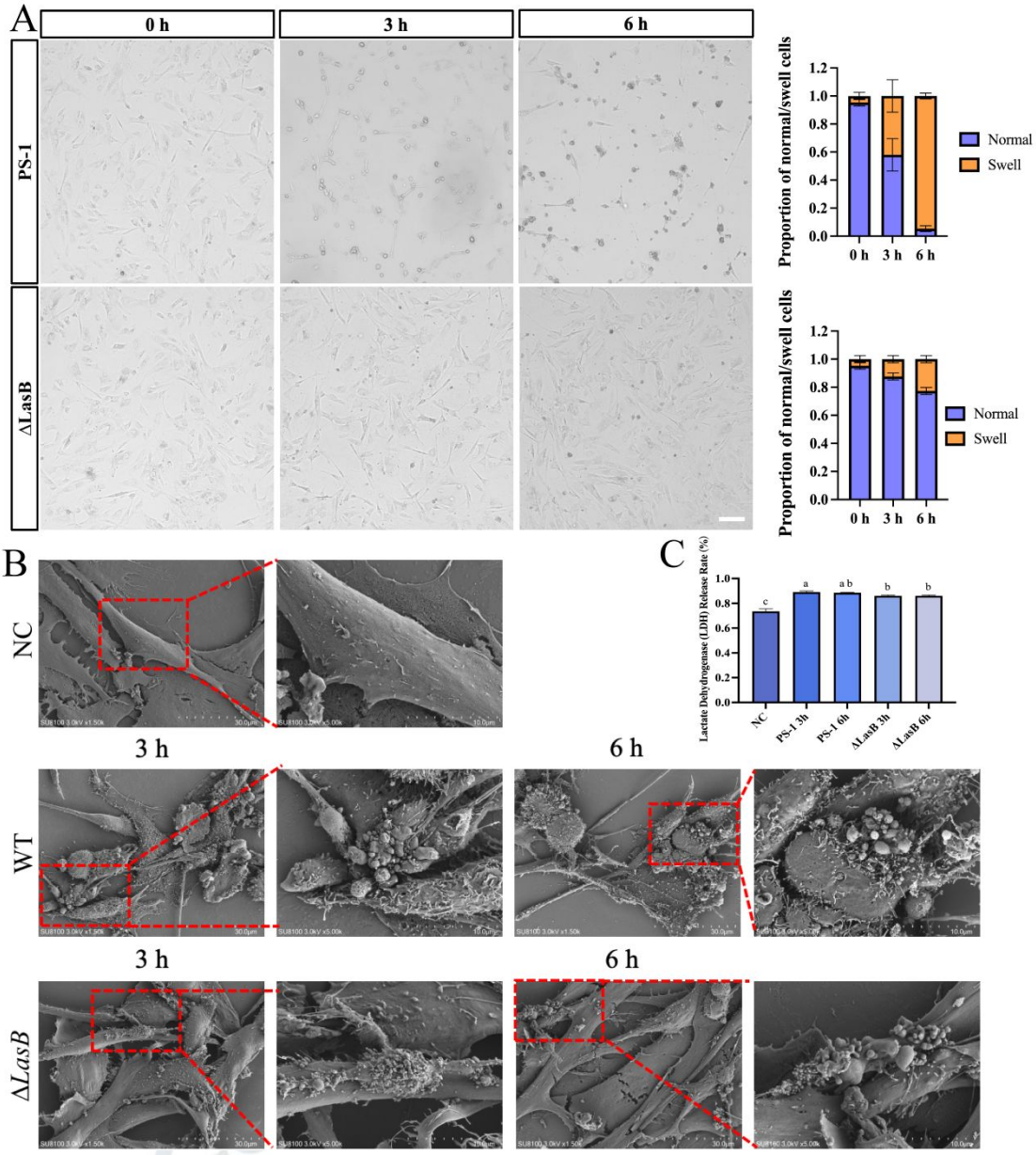
3.6 LasB mediated pyroptosis of *P. Sinensis* intestinal fibroblast-like cell

After determining that the inflammation in the intestine of *P. Sinensis* infected with ΔLasB would be reduced, we aimed to investigate the effect of LasB on the intestinal fibroblast-like cells of *P. Sinensis* at the cellular level. In our previous work, we have successfully established intestinal fibroblast-like cells from *P. Sinensis*. For the cell infection, the intestinal fibroblast-like cells were cultured to a confluence of 90%, and then PS-1 was introduced at a bacterial to cell ratio (MOI) of 1:1. Samples were collected at specific time points for observation under a regular optical microscope and for scanning electron microscopy imaging. The results from the regular optical microscope and scanning electron microscopy showed that after infection with PS-1, a few cells exhibited changes in morphology as early as 3 h post-infection, such as slight damage to the cell membrane or reduced cell-to-cell contact. At 6 h post-infection, the changes in cell morphology were more pronounced, with more cell damage observed, including cell membrane rupture, leakage of cell contents, and cell aggregation or detachment. Although there might have been some changes in cell morphology at 6 h post-infection, the degree of cell damage was milder, and the integrity and distribution of the cells were relatively better compared to the PS-1 group (Fig. 6A and 6B). Quantitative analysis of cell morphology revealed that PS-1 induced rapid and severe cellular swelling thereafter. By 3 h, swollen cells in the WT group reached 42.0%, and by 6 h, this proportion surged to 94.6%, leaving only 5.3% of cells morphologically intact. Conversely, the ΔLasB elicited

Uncorrected proof

significantly weaker morphological damage. The ΔLasB-infected cells largely retained normal morphology at 3 h (87.6%), and the swollen cell population was restricted to merely 22.6% even at 6 h. We preliminarily tested the release of lactate dehydrogenase (LDH), an indicator of cell membrane integrity that can serve as an auxiliary detection marker for pyroptosis (Fig. 6C). PS-1 infection significantly elevated LDH release to 0.89 ± 0.01% at 3 h and 6 h compared to the control group (0.74 ± 0.02%; $p < 0.05$). However, ΔLasB significantly attenuated this cellular damage, with the ΔLasB group maintaining a reduced LDH release of 0.86 ± 0.01% at both time points ($p < 0.05$). These results further illustrated that ΔLasB exhibited a significant reduction in its ability to induce cellular pyroptosis. These results indicated that PS-1 induced a pyroptosis-like cell death phenotype in *P. sinensis* fibroblast-like cells, and that LasB was closely associated with this pyroptotic phenotype.

uncorrected proof



554

555 **Fig. 6 LasB was associated with pyroptosis on the intestinal fibroblast-like cells of *P.***
556 ***Sinensis.*** A: Morphological changes of intestinal cells in *P. sinensis* treated with PS-1 and ΔLasB
557 (Light microscopy, 10X). Scale bar, 50 μm. B: Morphological changes of intestinal cells in *P.*
558 *sinensis* treated with PS-1 and ΔLasB (Electron microscopy). C: LDH release rate in intestinal
559 cells of *P. sinensis* treated with PS-1 and ΔLasB. Scale bar 30/10 μm.

560 **3.7 Transcriptomic analysis of *P. sinensis* intestinal fibroblast-like cells infected**
561 **with *A. hydrophila* PS-1 (WT) or ΔLasB (KOL) strain**

562 To investigate the role of LasB in host–pathogen interactions, *P. sinensis*
563 intestinal fibroblast-like cells were infected with *A. hydrophila* wild-type strain
564 (WT/PS-1) or the ΔLasB strain (KOL), followed by transcriptomic analysis. At 3 h
565 post-infection, the volcano plot (Fig. 7A) showed a distinct transcriptional profile
566 between ΔLasB and PS-1 infected cells. Compared with WT, KOL infection resulted

in a reduced number and magnitude of significantly upregulated genes, while a subset of genes was downregulated, indicating that LasB contributes to early host transcriptional activation. At 6 h post-infection, this difference became more pronounced (Fig. 7C), with WT infection inducing a larger set of differentially expressed genes (DEGs), particularly genes associated with inflammatory and stress responses, whereas KOL infection elicited a comparatively attenuated response. Gene Ontology (GO) and Kyoto Encyclopedia of Genes and Genomes (KEGG) enrichment analysis of DEGs at 3 h post-infection revealed that WT-induced genes were mainly enriched in biological processes related to immune response, inflammatory signaling, cell death, and response to stimulus (Fig. 7B and S2). In contrast, KOL infection showed weaker enrichment in these categories. At 6 h post-infection, DEGs were significantly enriched in pathways associated with cytokine-mediated signaling, regulation of programmed cell death, and innate immune responses, with WT-infected cells again displaying stronger enrichment intensity than KOL-infected cells (Fig. 7D and S2). These results suggest that LasB plays an important role in amplifying host immune and cell death–related pathways during infection.

A heatmap of the top 50 DEGs across all groups (Fig. 7E) demonstrated clear clustering according to infection type and time point. WT-infected samples showed robust upregulation of a distinct gene set compared with KOL-infected samples, while KOL infection maintained expression patterns closer to the control condition. This global expression pattern further supports the notion that LasB significantly modulates host transcriptional responses. In (Fig. 7F), we selected pyroptosis pathway-related genes, including *IL-1β*, *NLRP3*, *GSDMA*, *IL18*, *GSDME*, *ASC*, *GSDMD*, and *Caspase-1*, for heatmap analysis. The results showed that the expression of genes such as GSDMA and NLRP3 significantly decreased after LasB knockout. To further validate the activation of the pyroptosis pathway, the mRNA expression levels of key related genes were quantified via RT-qPCR. Consistent with the heatmap analysis, wild-type PS-1 infection significantly upregulated the expression of core pyroptosis executors and sensors, particularly *GSDMA* (1.42-fold) and *NLRP3* (1.61-fold), compared to NC group. Similar striking upregulations were observed for downstream inflammatory cytokines including *IL-1β* (1.65-fold) and *IL-18* (1.92-fold). Crucially, knocking out LasB largely reversed this transcriptional activation. In the ΔLasB-infected group, the expression levels of *GSDMA* and *NLRP3* were markedly reduced to 1.25-fold and 1.33-fold, respectively. A corresponding

Uncorrected proof

601 downregulation was also observed for *IL-1β*, *IL-18*, and *Caspase-1*, whereas the
602 expression of *GSDME* remained relatively stable across all treatments (Fig. S3).
603 These quantitative results robustly confirm that the PS-1-triggered upregulation of the
604 NLRP3/GSDMA pyroptosis axis is highly dependent on the virulence factor LasB.

605 To further validate the role of LasB in mediating pyroptosis in *P. sinensis*, we
606 performed immunohistochemistry (IHC) on intestinal sections using anti-GSDMA
607 and anti-Caspase-1 antibodies. The results revealed that both GSDMA and Caspase-1
608 were highly expressed in the intestinal tissues following wild-type PS-1 infection. In
609 contrast, infection with the ΔLasB mutant resulted in a significant downregulation of
610 GSDMA and Caspase-1 expression. Collectively, these findings demonstrate that
611 LasB drives GSDMA-dependent pyroptosis (Fig. S4). Collectively, these findings
612 elucidate the molecular mechanism underlying the observed intestinal tissue damage,
613 establishing LasB-dependent pyroptosis as a central pathogenic mechanism of
614 bacterial enteritis in *P. sinensis*.

615 To verify the direct effect of LasB protein on *P.sinensis* intestinal fibroblast-like
616 cells, concentration gradient treatment groups (1, 5, 10, and 20 μg) were established,
617 with NC (negative control) and PBS (solvent control) as controls, and cell
618 morphological changes were observed at 0 h, 3 h, and 6 h. The results showed that
619 compared with the NC and DPBS groups, all LasB protein treatment groups (1-20 μg)
620 showed no obvious morphological changes at 0 h, 3 h, and 6 h. Cells maintained
621 normal adherent status, and no characteristic pyroptosis changes such as obvious
622 membrane bubbling, swelling, content leakage, or cell detachment were observed.
623 Cell confluency remained essentially comparable to the control groups at all time
624 points (Fig. S5). Therefore, extracellular addition of recombinant LasB protein alone
625 cannot induce pyroptosis, suggesting that LasB may need to enter cells in a bacterial
626 secretion-dependent manner to exert cytotoxic effects.
627

Uncorrected proof

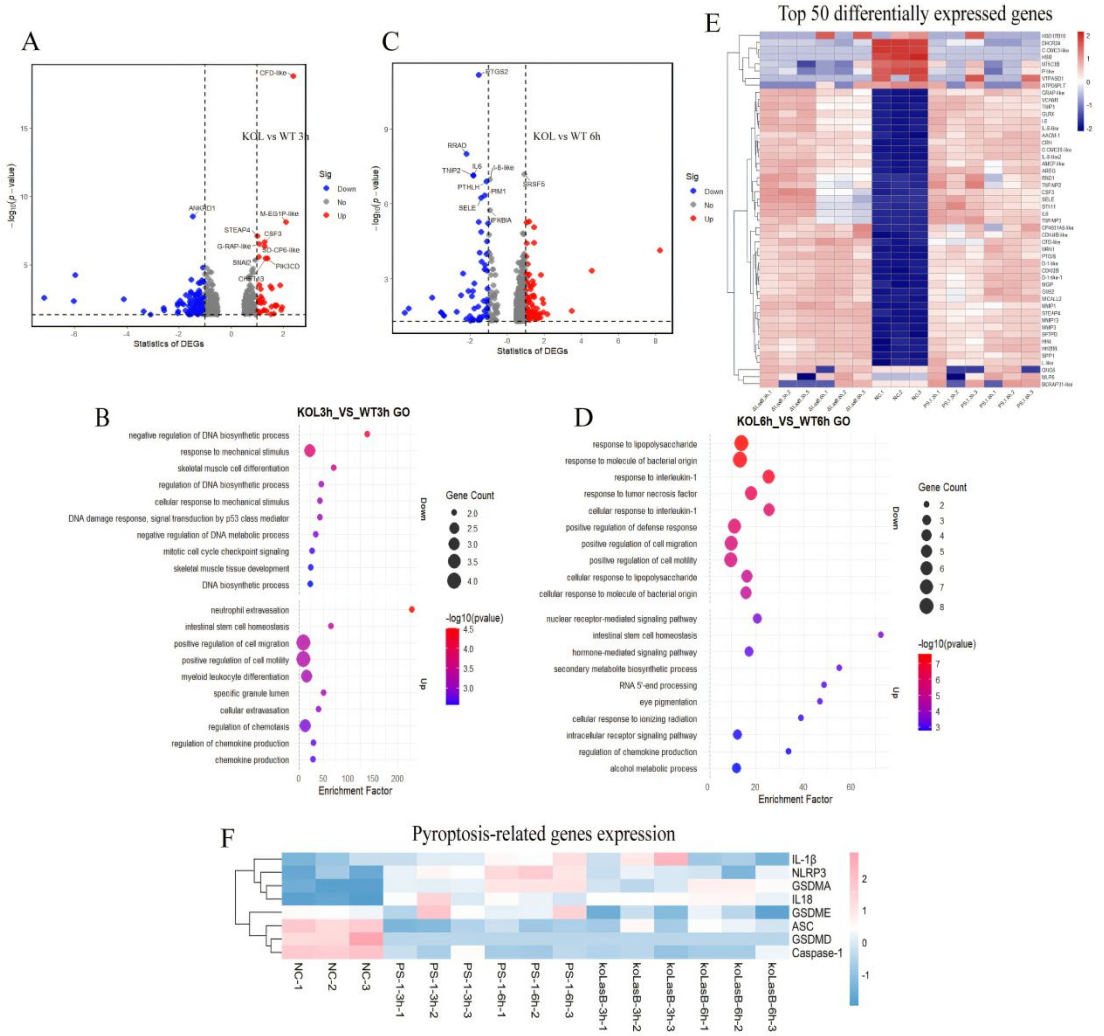


Fig. 7 Transcriptomic analysis of *P. sinensis* intestinal fibroblast-like cells infected with *A. hydrophila* PS-1 or ΔLasB strain. A: Volcano plot showing DEGs between KOL- and WT-infected cells at 3 h post-infection. Red and blue dots represent significantly upregulated and downregulated genes, respectively, while gray dots indicate non-significant genes. B: GO enrichment analysis of DEGs at 3 h post-infection, highlighting major biological processes affected by WT and KOL infection. C: Volcano plot of DEGs between KOL- and WT-infected cells at 6 h post-infection. D: GO enrichment analysis of DEGs at 6 h post-infection. E: Heatmap of the top 50 DEGs across different infection groups and time points, illustrating global transcriptional differences induced by WT and KOL strains. F: Heatmap of pyroptosis-related genes showing that WT infection markedly upregulates pyroptosis-associated pathways, whereas LasB knockout significantly attenuates this response, indicating that LasB is a key mediator of host cell pyroptosis.

4 Discussion

In this study, we systematically characterized the LasB protease of *A. hydrophila* PS-1 and demonstrated that it functioned as a temperature-dependent virulence

determinant during infection of *P. sinensis*. We found that LasB expression peaked at 35℃, and that LasB was a host-induced secreted protein released extracellularly predominantly in a cleaved form (35 kDa). By constructing a LasB deletion mutant (ΔLasB) and assessing its phenotype in vivo and in vitro, we further confirmed that LasB contributed substantially to bacterial pathogenicity. Specifically, LasB promoted intestinal inflammation and was associated with a pronounced pyroptosis-like phenotype in intestinal fibroblast-like cells, whereas deletion of LasB markedly attenuated virulence, reduced tissue damage, and alleviated inflammatory injury. Collectively, these findings supported the conclusion that LasB was a key effector mediating the high-temperature pathogenicity of strain PS-1, providing a mechanistic entry point for understanding temperature-driven outbreaks and identifying potential targets for intervention.

A major observation in our fibroblast-like cell infection assays was that LasB robustly correlated with pyroptosis-associated cellular outcomes, suggesting that LasB may modulate inflammasome-related pathways in the host. At present, however, this conclusion was primarily based on cellular phenotypes, and molecular validation remains necessary. Previous work on *P. aeruginosa* had shown that its LasB could directly activate IL-1β, a pivotal cytokine linked to inflammasome signaling and pyroptosis (Sun et al., 2020). In addition, Duan et al. (2023) reported that quorum sensing–regulated LasB could cleave death domains of innate immune adaptor proteins such as ASC and MyD88, thereby dampening host immune responses and enhancing bacterial persistence. These studies collectively indicated that LasB-family proteases may exert multifaceted immunomodulatory effects that depended on infection context, host cell type, and bacterial regulatory state. Interestingly, such immunomodulation could theoretically produce either suppression or enhancement of pyroptosis depending on whether inflammasome assembly and upstream signaling were inhibited, or whether inflammatory cytokines and danger signaling are amplified. Therefore, although our data supported a strong association between LasB and pyroptosis-like injury, the precise directionality and molecular route by which PS-1 LasB influenced inflammasome activation require careful dissection. Mechanistically, sequence analysis indicated that the LasB M23 domain was conserved across diverse bacteria, consistent with the broader functional repertoire of

Uncorrected proof

677 M23 metalloproteases as both peptidoglycan remodelers and virulence-associated
678 factors. Members of the M23 family have been implicated not only in bacterial
679 physiology but also in immune evasion and tissue invasion (Everett et al., 2021). For
680 example, *Staphylococcus aureus* LytM was not only a "Gly-Gly bond" hydrolase but
681 also a dual-specificity endopeptidase that cleaved the "D-Ala-Gly cross-link bond".
682 This function enabled it to play a central role in the maturation, remodeling of *S.*
683 *aureus* peptidoglycan, and resistance to exogenous PG hydrolase attacks (Antenucci
684 et al., 2024). Likewise, Enterococcus faecalis GelE had been shown to degrade fibrin,
685 alter biofilm structure, facilitate dissemination, and interfere with innate immune
686 responses such as neutrophil chemotaxis (Thurlow et al., 2010). Given these
687 precedents, it was plausible that PS-1 LasB might facilitate pathogenesis through (i)
688 direct tissue matrix and barrier disruption, (ii) modulation of immune signaling
689 adaptors, and/or (iii) shaping inflammatory cytokine activation, ultimately
690 contributing to intestinal inflammation and pyroptosis-associated pathology. In future
691 work, targeted assays should be performed to assess inflammasome pathway
692 activation, including measurement of IL-1β maturation, caspase-1 activity, gasdermin
693 cleavage, and ASC speck formation, coupled with inhibitor- or knockdown-based
694 validation to establish causality.

695 Another notable finding was that LasB was secreted predominantly as a ~35 kDa
696 cleaved product, suggesting that PS-1 LasB undergoed extracellular maturation or
697 processing during secretion. To our knowledge, similar cleavage behavior has not
698 been systematically described for *A. hydrophila* LasB in the context of
699 temperature-regulated virulence, and this processing event might be linked to the
700 increased secretion observed at elevated temperature (Kessler et al., 1998). One
701 reasonable hypothesis was that a temperature-responsive bacterial protease (or a
702 secretion-associated processing mechanism) cleaves the LasB precursor, producing
703 the mature extracellular form with altered stability, activity, or substrate specificity.
704 To test this hypothesis, subsequent studies should (i) identify interacting partners and
705 candidate processing enzymes using co-immunoprecipitation or affinity purification
706 coupled with mass spectrometry, (ii) map the cleavage site(s) by N-terminal
707 sequencing or proteomic peptide mapping, and (iii) determine whether cleavage was
708 required for enzymatic activity and virulence phenotypes by constructing
709 cleavage-site mutants. Establishing a temperature-dependent processing mechanism
710 would not only expand our understanding of LasB maturation, but also provide a

Uncorrected proof

broader framework for investigating how environmental cued modulate protease-mediated virulence in *Aeromonas*.

The temperature-dependent expression and processing of LasB, which yields a highly active ~35 kDa mature form at 35℃, not only elucidate the molecular basis of high-temperature pathogenesis in *A. hydrophila* but also present a promising target for disease intervention in *P. sinensis*. Because the M23 metalloprotease domain is highly conserved and serves as a core effector driving host pyroptosis and inflammatory injury, mature LasB represents an ideal candidate for vaccine development (Konkel et al., 2000). Traditional inactivated vaccines often exhibit reduced efficacy during peak summer months due to the low abundance of such conditionally expressed virulence factors. By developing targeted subunit or toxoid vaccines based on mature LasB, robust neutralizing antibodies can be stimulated to specifically block its catalytic activity during infection. Furthermore, taking advantage of this temperature-dependent mechanism, vaccination programs can be strategically scheduled during late spring (e.g., 25-28℃), enabling the host to establish optimal immunity before the water temperature reaches the 35℃ danger zone where LasB expression surges. Ultimately, this targeted and temperature-guided immunization strategy will offer a practical approach to preemptively intercepting severe summer disease outbreaks in aquaculture.

Taken together, using *A. hydrophila* PS-1 isolated from *P. sinensis* as a model, we delineated a central role for LasB in temperature-dependent host–pathogen interactions. We demonstrated that LasB was maximally expressed at 35℃, was induced by host intestinal components, and was secreted as a ~35 kDa processed form. Loss of LasB substantially reduced virulence in vivo, mitigated intestinal inflammation, and diminished pyroptosis-like injury in intestinal fibroblast-like cells. Importantly, our findings provided evidence that LasB acted as a temperature-responsive effector contributing to bacterial enteritis in *P. sinensis*. This work offers both fundamental insights and practical guidance for controlling temperature-regulated disease outbreaks in aquaculture.

Uncorrected proof

SUPPLEMENTARY DATA

Supplementary data to this article can be found online.

COMPETING INTERESTS

The authors declare that they have no competing interests.

AUTHORS' CONTRIBUTIONS

C.S.Y.: Conceptualization, methodology, investigation, formal analysis, writing (original draft), visualization. C.S.Y. designed and performed the majority of experiments and data analysis, and prepared the original manuscript.

D.F.: Conceptualization, methodology, resources, writing (review and editing), supervision, funding acquisition. D.F. conceived the research, designed the experimental framework, provided key resources, supervised the study, and edited the manuscript.

H.Z.J.: Investigation, formal analysis. H.Z.J. performed sequence analysis, phylogenetic reconstruction, and assisted with transcriptomic data interpretation.

W.X.Q.: Investigation. W.X.Q. conducted primary cell culture and cell infection assays.

X.J.H. and S.W.: Investigation, methodology. X.J.H. and S.W. contributed to experimental execution and data collection.

G.C.T.: Conceptualization, resources, writing (review and editing), supervision, funding acquisition, project administration. G.C.T. co-supervised the research, provided infrastructure, critically revised the manuscript, and administered the project.

ETHICS STATEMENT

All the animal experiments were carried out according to a protocol approved by the Experimental Animal Ethics Committee of Zhejiang Wanli University, China (Approval number: 20241017001). Animals were housed under standard aquaculture conditions with appropriate water temperature, pH, and feeding regimens to minimize stress and suffering. For infection experiments, turtles were monitored daily, and humane endpoints were established to ensure that animals exhibiting severe clinical

uncorrected proof

signs (e.g., inability to swim, extensive ulceration, or moribund state) were euthanized immediately by cervical dislocation or anesthetic overdose to prevent unnecessary suffering.

References

Abdella B, Abozahra NA, Shokrak NM, et al. 2023. Whole spectrum of *Aeromonas hydrophila* virulence determinants and the identification of novel SNPs using comparative pathogenomics. Scientific Reports, 13(1): 19854. DOI: 10.1038/s41598-023-34887-1

Abdella B, Shokrak NM, Abozahra NA, et al. 2024. Aquaculture and *Aeromonas hydrophila*: a complex interplay of environmental factors and virulence. Aquaculture International, 32(6): 7671–7681. DOI: 10.1007/s10499-024-01535-y

Antenucci L, Virtanen S, Thapa C, et al. 2024. Reassessing the substrate specificities of the major *Staphylococcus aureus* peptidoglycan hydrolases lysostaphin and LytM. eLife, 13: RP93673. DOI: 10.7554/eLife.93673

Awan F, Dong Y, Liu J, et al. 2018. Comparative genome analysis provides deep insights into *Aeromonas hydrophila* taxonomy and virulence-related factors. BMC Genomics, 19(1): 712. DOI: 10.1186/s12864-018-5100-4

Cascarano MC, Stavrakidis-Zachou O, Mladineo I, et al. 2021. Mediterranean aquaculture in a changing climate: temperature effects on pathogens and diseases of three farmed fish species. Pathogens, 10(9): 1205. DOI: 10.3390/pathogens10091205

Chen CS, Guo ML, Wei K, et al. 2017. Study on preventive effect of cecropin and lysozyme on skin fester disease of *Trionyx sinensis*. Sichuan Journal of Zoology, 36(3): 311-316 (In Chinese). DOI: 10.11984/j.issn.1000-7083.20160368

Chen H, Huang Y, Liu T, et al. Characteristics of seasonal spermatogenesis in the soft-shelled turtle. Anim Reprod Sci. 2020 Mar;214:106307. Doi: 10.1016/j.anireprosci.2020.106307

Dai F, Chen S, Sun W, et al. 2026. Identification of *Aeromonas hydrophila* PS-1 and GFP-labeled tracking of its infection in *Pelodiscus sinensis*. Aquaculture, 610. DOI: 10.1016/j.aquaculture.2025.742914

Dai XL, Lü SJ, Liu L, et al. 2025. Therapeutic effects of echinacea purpurea polysaccharide on viral parotitis in the Chinese Soft-Shelled Turtle (*Trionyx sinensis*). Progress in Fishery Sciences:

Uncorrected proof

807 46(6): 261-270 (In Chinese). DOI: 10.3969/j.issn.2095-9869.20241124001
808 De Silva LADS, Wickramanayake MVKS, Heo GJ. 2021. Virulence and antimicrobial resistance
809 potential of *Aeromonas spp*. associated with shellfish. Letters in Applied Microbiology, 73(2):
810 176-186. DOI: 10.1111/lam.13489
811 Deng W, Bai Y, Deng F, et al. 2022. *Streptococcal pyrogenic* exotoxin B cleaves GSDMA and
812 triggers pyroptosis. Nature, 602(7897): 496-502. DOI: 10.1038/s41586-021-04384-4
813 Duan X, Boo ZZ, Chua SL, et al. 2023. A bacterial quorum sensing regulated protease inhibits
814 host immune responses by cleaving death domains of innate immune adaptors. Advanced Science,
815 10(34): e2304891. DOI: 10.1002/advs.202304891
816 Everett MJ, Davies DT. 2021. *Pseudomonas aeruginosa* elastase (LasB) as a therapeutic target.
817 Drug Discovery Today, 26(9): 2108-2123. DOI: 10.1016/j.drudis.2021.02.026
818 Fernández-Bravo A, Figueras MJ. 2020. An update on the genus *Aeromonas*: taxonomy,
819 epidemiology, and pathogenicity. Microorganisms, 8(1): 129. DOI:
820 10.3390/microorganisms8010129
821 Fikri F, Wardhana DK, Purnomo A, et al. 2022. Aerolysin gene characterization and antimicrobial
822 resistance profile of *Aeromonas hydrophila* isolated from milkfish (*Chanos chanos*) in Gresik,
823 Indonesia. Veterinary World, 15(7): 1759-1764. DOI: 10.14202/vetworld.2022.1759-1764
824 Guo H, Xia Z, Tang W, et al. 2016. Establishment and characterization of a cell line from the
825 Chinese soft-shelled turtle *Pelodiscus sinensis*. In Vitro Cellular & Developmental
826 Biology-Animal, 52(6): 673-682. DOI: 10.1007/s11626-016-0015-3
827 He RZ, Liang QR, Tian QQ, et al. 2025. Disease surveillance and control suggestions for
828 cultivating *Larimichthys crocea* in Zhejiang Province from 2018 to 2023. Zhejiang Agricultural
829 Sciences, 66(10): 2473-2477 (In Chinese). DOI: 10.16178/j.issn.0528-9017.20240978
830 Jiang R, Zhang J, Liao Z, et al. 2023. Temperature-regulated type II grass carp reovirus establishes
831 latent infection in *Ctenopharyngodon idella* brain. Virologica Sinica, 38(3): 440-447. DOI:
832 10.1016/j.virs.2023.04.006
833 Kessler E, Safrin M, Gustin JK, Ohman DE. 1998. Elastase and the LasA protease of
834 Pseudomonas aeruginosa are secreted with their propeptides. Journal of Biological Chemistry,
835 273(46): 30225-30231. DOI: 10.1074/jbc.273.46.30225
836 Konkel ME, Tilly K. 2000. Temperature-regulated expression of bacterial virulence genes.

Uncorrected proof

837 Microbes and Infection, 2(2): 157-166. DOI: 10.1016/S1286-4579(00)00272-0
838 Li H, Yu S, Ye WQ, et al. 2025. Research on comprehensive prevention and control of ulcerative
839 skin disease in *Pelodiscus sinensis* farming. Hebei Fisheries, (10): 27-30 (In Chinese). DOI:
840 10.3969/j.issn.1004-6755.2025.10.007
841 Lin X, Huang HY, Zhou JW. 2005. Preliminary study of specific egg-yolk-antibody in preventing
842 soft-shelled turtle from red neck disease. Chinese Journal of Fisheries, 18(1): 56-60 (In Chinese).
843 DOI: 10.3969/j.issn.1005-3832.2005.01.012
844 Pattanayak S, Priyadarsini S, Paul A, et al. 2020. Diversity of virulence-associated genes in
845 pathogenic *Aeromonas hydrophila* isolates and their in vivo modulation at varied water
846 temperatures. Microbial Pathogenesis, 147: 104424. DOI: 10.1016/j.micpath.2020.104424
847 Sun J, LaRock DL, Skowronski EA, et al. 2020. The *Pseudomonas aeruginosa* protease LasB
848 directly activates IL-1β. EBioMedicine, 60: 102984. DOI: 10.1016/j.ebiom.2020.102984
849 Thomas SG, Glover MA, Parthasarathy A, et al. 2020. Expression of a *Shiga*-like toxin during
850 plastic colonization by two multidrug-resistant bacteria, *Aeromonas hydrophila* RIT668 and
851 Citrobacter freundii RIT669, isolated from endangered turtles (*Clemmys guttata*).
852 Microorganisms, 8(8): 1172. DOI: 10.3390/microorganisms8081172
853 Thurlow LR, Thomas VC, Narayanan S, et al. 2010. Gelatinase contributes to the pathogenesis of
854 endocarditis caused by *Enterococcus faecalis*. Infection and Immunity, 78(11): 4936-4943. DOI:
855 10.1128/IAI.01118-09
856 Wu X, Xu XL, Kan Z, et al. 2024. Current situation and outlook about *Trionyx Sinensis*
857 aquaculture industry of China. Science and Technology of Tianjin Agriculture and Forestry, (6):
858 39-42 (In Chinese). DOI: 10.3969/j.issn.1002-0659.2024.06.012
859 Xiang J, Chen XW, Huang JZ, et al. 2025. Application of microecological preparations in healthy
860 aquaculture of *Trionyx sinensis*. Contemporary Fisheries, 50(9): 73-75 (In Chinese). DOI:
861 10.3969/j.issn.1674-9049.2025.09.034
862 Chen S, Zhou Y, Chen Y, et al. 2018. Fastp: an ultra-fast all-in-one FASTQ preprocessor.
863 Bioinformatics, 34(17): i884-i890. DOI: 10.1093/bioinformatics/bty560
864 Pertea M, Kim D, Pertea GM, et al. 2016. Transcript-level expression analysis of RNA-seq
865 experiments with HISAT, StringTie and Ballgown. Nature Protocols, 11(9): 1650-1667. DOI:
866 10.1038/nprot.2016.095

Uncorrected proof

867 Kim D, Langmead B, Salzberg SL. 2015. HISAT: a fast spliced aligner with low memory
868 requirements. Nature Methods, 12(4): 357-360. DOI: 10.1038/nmeth.3317
869 Pertea M, Pertea GM, Antonescu CM, et al. 2015. StringTie enables improved reconstruction of a
870 transcriptome from RNA-seq reads. Nature Biotechnology, 33(3): 290-295. DOI:
871 10.1038/nbt.3122
872 Soneson C, Love MI, Robinson MD. 2016. Differential analyses for RNA-seq: transcript-level
873 estimates improve gene-level inferences. F1000Research, 4: 1521. DOI:
874 10.12688/f1000research.7563.2

uncorrected proof

uncorrected proof